Article

Asymmetric hydrogenation of ketimines with minimally different alkyl groups

https://doi.org/10.1038/s41586-024-07581-z

Received: 1 March 2024

Accepted: 17 May 2024

Published online: 28 May 2024

Check for updates

Mingyang Wang[1,6], Shihan Liu[2,6], Hao Liu[1,6], Yujie Wang[1], Yu Lan[3,4,5]✉ & Qiang Liu[1]✉

Asymmetric catalysis enables the synthesis of optically active compounds, often requiring the differentiation between two substituents on prochiral substrates[1]. Despite decades of development of mainly noble metal catalysts, achieving differentiation between substituents with similar steric and electronic properties remains a notable challenge[2,3]. Here we introduce a class of Earth-abundant manganese catalysts for the asymmetric hydrogenation of dialkyl ketimines to give a range of chiral amine products. These catalysts distinguish between pairs of minimally differentiated alkyl groups bound to the ketimine, such as methyl and ethyl, and even subtler distinctions, such as ethyl and *n*-propyl. The degree of enantioselectivity can be adjusted by modifying the components of the chiral manganese catalyst. This reaction demonstrates a wide substrate scope and achieves a turnover number of up to 107,800. Our mechanistic studies indicate that exceptional stereoselectivity arises from the modular assembly of confined chiral catalysts and cooperative non-covalent interactions between the catalyst and the substrate.

A central objective in asymmetric catalysis is creating stereoselective catalysts that can distinguish between prochiral faces or centres, especially in reactions such as nucleophilic additions to unsaturated double bonds[1] (Fig. 1a). Although most efforts have focused on substrates containing aryl and alkyl groups, achieving high enantioselectivity remains challenging when substituents possess similar steric and electronic properties[4–6], such as primary alkyl and methyl groups[7–13]. A notable example includes the 'methyl, ethyl' pairing, addressed in recent studies[2,3]. However, distinguishing between two primary alkyl groups is more difficult. Developing a universal method that addresses not only the 'methyl, ethyl' pair but also more intricate combinations such as 'ethyl, *n*-propyl' and '*n*-propyl, *n*-pentyl' remains a challenge in asymmetric catalysis[14–16].

In traditional approaches, chiral catalysts primarily leverage steric interactions between the catalyst and the substrate to influence stereoselectivity. Yet, emerging studies highlight the critical role of non-covalent interactions in shaping this selectivity[17]. Mirroring enzymes of nature, which exert precise control over organic transformations through confined active sites and a series of secondary interactions[18], synthetic strategies have evolved. These enzymes stabilize transition states in a manner that often surpasses synthetic catalysts, aided by the fine-tunability of their active sites through protein engineering[19–21]. Inspired by this, we designed chiral catalysts with confined, modularly assembled reactive sites, enabling non-covalent interactions with substrates similar to enzymatic function[22–24]. This approach markedly enhances the tunability of the catalyst beyond traditional metal–ligand systems, prospectively addressing persistent challenges such as the enantioselective hydrogenation of ketimines with two primary alkyl groups.

The asymmetric hydrogenation of imines represents a highly efficient route to synthesize chiral amines[25–29], essential in numerous active pharmaceutical ingredients and bioactive molecules. Compared with other existing approaches[30–33], this method stands out for its remarkable substrate scope and functional group tolerance, thereby granting access to a broader chemical space. However, challenges persist for the reactions of dialkyl ketimines, notably the rapid equilibrium between *E*- and *Z*-stereoisomers and their tautomerization into four potential enamine intermediates under typical reaction conditions. These issues often trigger complex reaction pathways that produce enantiomeric products with reduced enantioselectivity (Fig. 1b). Our innovative catalyst design uses the anionic metal hydride complex rather than the traditional neutral metal hydride species to activate the ketimine substrate more effectively through cooperative hydrogen bonding and coordination interactions. This strategic switch prevents the competitive hydrogenation of electron-rich enamine species and suppresses undesired pathways. This adjustment also facilitates selective ketimine hydrogenation under mild conditions favourable for enantiocontrol, because of the enhanced nucleophilicity of anionic metal hydride complexes[34,35]. The modular assembly of the catalyst from a chiral anionic ligand, a suitable countercation and a solvent cluster around the countercation enhances the enantio-recognition of different primary alkyl substituents (Fig. 1c). Supported by advancements in Earth-abundant-metal-catalysed asymmetric hydrogenation[26,27,33,36,37], particularly the emerging of manganese hydride catalysis[29,38], we introduce a class of confined, modularly assembled anionic manganese hydride catalysts[39]. These catalysts enable the enantioselective hydrogenation of dialkyl ketimines with a wide substrate scope and a high turnover number (Fig. 1d).

[1]Center of Basic Molecular Science (CBMS), Department of Chemistry, Tsinghua University, Beijing, China. [2]College of Chemistry and Molecular Sciences, Henan University, Kaifeng, China. [3]School of Chemistry and Chemical Engineering, Chongqing Key Laboratory of Theoretical and Computational Chemistry, Chongqing University, Chongqing, China. [4]College of Chemistry, Pingyuan Laboratory, Zhengzhou University, Zhengzhou, Henan, China. [5]Pingyuan Laboratory, Xinxiang, Henan, China. [6]These authors contributed equally: Mingyang Wang, Shihan Liu, Hao Liu. ✉e-mail: lanyu@cqu.edu.cn; qiang_liu@mail.tsinghua.edu.cn

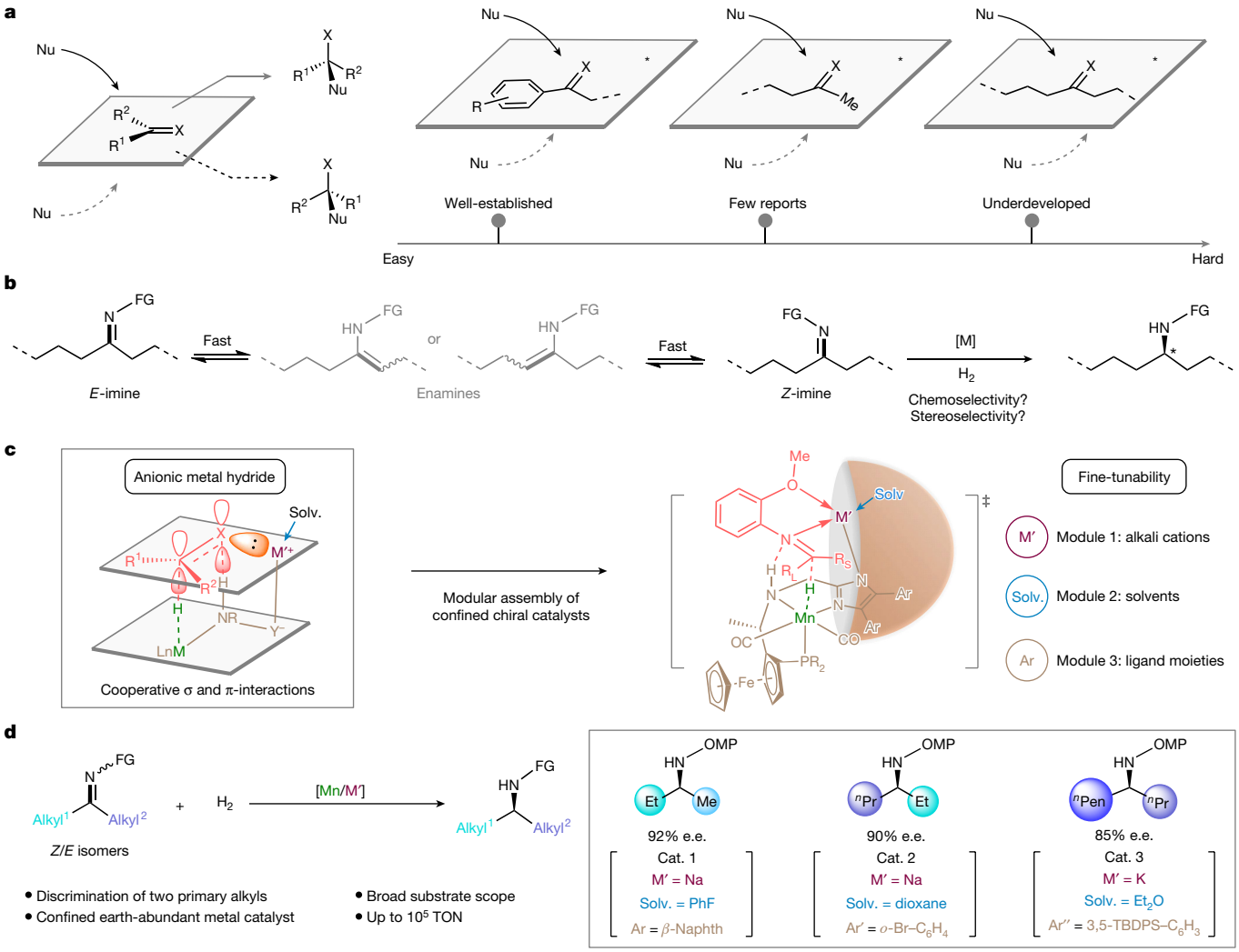

Fig. 1 | The distinction between two minimally differentiated alkyl groups. **a**, Stereocenter set by the distinction between two substituents in asymmetric catalysis. **b**, Fast equilibrium between *E*/*Z* isomers of dialkyl ketimines and enamines. **c**, Catalyst design, which introduces cooperative non-covalent attractive interactions and modular assembly of confined reaction sites towards a precise stereoselectivity control. **d**, The confined, chiral, Earth-abundant metal catalyst enables the accurate distinguishment between pairs of two primary alkyl groups in asymmetric hydrogenation of ketimines. FG, functional group; OMP = 2-methoxyphenyl; TBDPS = *tert*-butyldiphenylsilyl, Solv., solvent, TON, turnover number.

Reaction development

Following optimization of key reaction parameters, such as *N*-protecting groups, solvents and temperature (Supplementary Tables 1–3), we selected the ketimine **1a** (mixture of *Z*/*E* isomers in a ratio of 1:1) derived from 3-heptanone and *o*-methoxyaniline as the model substrate to initiate a systematic exploration of catalysts. Our focus was primarily on the 4,5-disubstituted imidazole units of the NNP pincer ligands (Fig. 2a), considering them crucial components of a confined reaction site with a notable impact on enantioselectivity. The enantiomeric excess (e.e.) of **2a** demonstrated a subtle dependence on the electronic properties of substituents on the aryl group, with a notable responsiveness to the substitution pattern on the aromatic group. Catalysts with substituents on *p*- or *m*-positions yielded poor results, with e.e. values ranging from 3% to 48%. Marked enhancements in enantioselectivity were observed when catalysts containing *ortho*-substituted aryl groups were used, with the catalyst **Mn-13** featuring an *o*-bromophenyl group providing the best outcome at 95% yield and 91% e.e. Apart from the substituents on the imidazole group, the choice of metal countercations and solvents also played a pivotal part in this reaction. Control experiments were conducted to validate the proposed cooperative catalysis. The addition of 8 mol% 15-crown-5 as a sodium cation trapping agent led to a substantial decrease in the enantioselectivity of **2a** to 46% (Fig. 2b, entry 2). Furthermore, substituting sodium *bis*(trimethylsilyl)amide (NaHMDS) with potassium *bis*(trimethylsilyl)amide (KHMDS) as the base resulted in a diminished e.e. of **2a** to 58% (Fig. 2b, entry 3). It was also observed that the e.e. value decreased with a change in the solvent (Fig. 2b, entry 4). These experiments supported the involvement of the countercation and solvent molecules, along with the ligand moieties in the confined reaction site, contributing to precise enantioinduction. Furthermore, enantioselectivity has a slight dependence on temperature. Lowering the temperature improves enantioselectivity, although this is accompanied by a modest reduction in yield (Supplementary Tables 6 and 7).

Mechanistic investigations

To gain more insights into the model of stereoselectivity control, density functional theory (DFT) calculations were conducted to explain the observed enantioselectivity in the crucial hydride transfer step. *E*/*Z* isomerization of dialkyl imines was considered to proceed with a lower energy barrier through base-assisted enamide–imine tautomerism (Supplementary Fig. 24). The rapid equilibrium between *E*/*Z* imine isomers enables only one isomer to participate in the hydrogenation

a

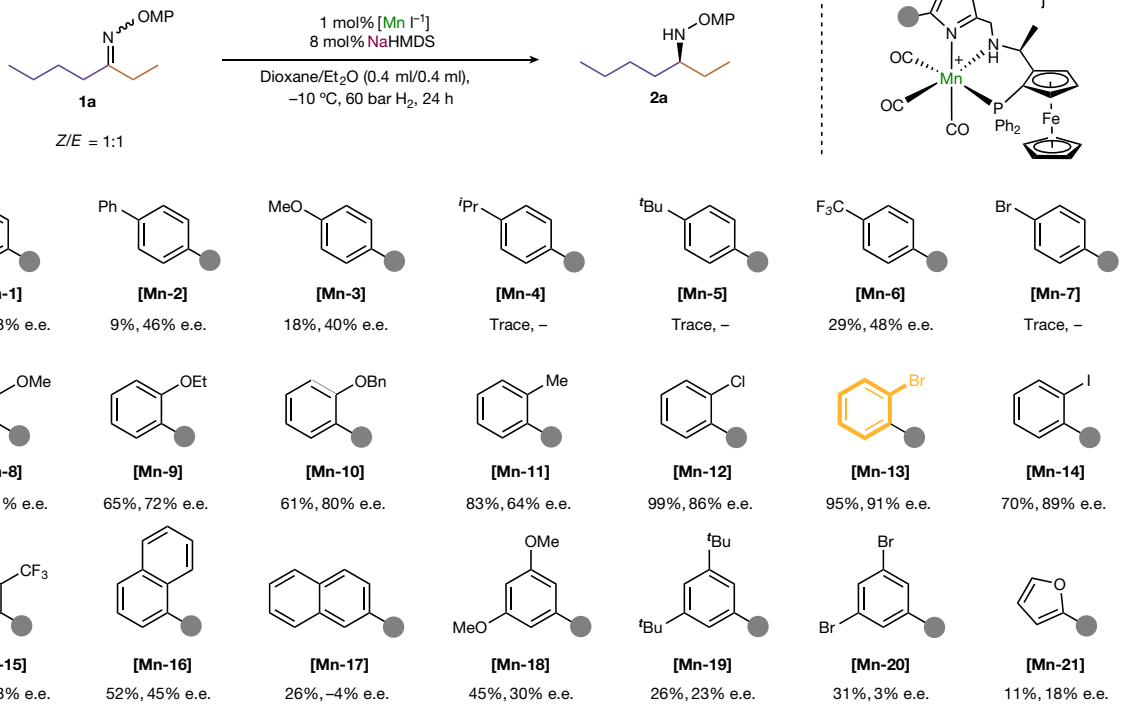

b

Entry	Variation of standard conditions	Yield (%)	e.e. (%)
1	None	95	91
2	8 mol% **15-crown-5** as additives	77	46
3	8 mol% **KHMDS** instead of **NaHMDS**	97	58
4	PhF as solvent	56	77

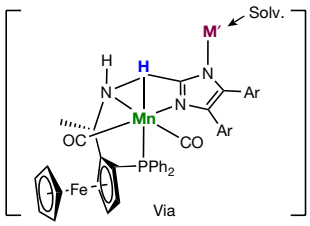

Fig. 2 | Optimization of reaction parameters. a, Screening of catalysts. The reactions were performed on a 0.25-mmol scale using 1 mol% [Mn], 1 mol% ligand and 8 mol% NaHMDS at −10 °C in a cosolvent of dioxane/Et_2O (0.4 ml/0.4 ml) for 24 h. The yields (%) were determined by gas chromatography analysis and enantioselectivities (% e.e.) were determined by chiral-phase high-performance liquid chromatography. **b**, Control experiments, including sodium cation capture, the change of base and solvent. OMP = 2-methoxyphenyl.

reaction following a favourable reaction pathway. Our study examined four substrate coordination forms with an anionic Mn–H complex, featuring a sodium countercation. In comparison to the stable chelating coordination between the sodium cation and the N and O atoms of the substrate, transition states involving cation–π interactions showed a substantial increase in energy barrier because of weaker coordination (Fig. 3a). Among the two superior transition states, ***Z-S*-TS$_4$** is favoured over ***E-R*-TS$_6$** by 2.2 kcal mol^{-1}, indicating the (*S*)-configured product **2a** as the predominant outcome, corroborated by experimental data. To gain a deeper understanding of the origin of enantioselectivity, a van der Waals surface map was used to analyse the hydride transfer transition states of ethyl *n*-butyl imine **1a** (Fig. 3b). The surface map for ***Z-S*-TS$_4$** shows that the small volume of the ethyl group fits well within the confined reaction site, facilitating the formation of the desired enantiomer. Conversely, in the unfavourable transition state ***E-R*-TS$_6$**, resulting in the opposite enantiomer, the larger volume of the *n*-butyl group challenges accommodation within the same space (Fig. 3b). These results underscore that the high stereoselectivity derives from the modular assembly of confined chiral catalysts and their cooperative non-covalent interactions with the substrate. A similar pattern is observed with a potassium cation, which shows a smaller activation energy difference of 1.3 kcal mol^{-1} because of its larger ionic radius (Fig. 3c). Enlarged chiral confinement shaped by the potassium cation, compared with sodium, ultimately results in poorer enantioselectivity, illustrating the marked impact of the countercation on enantio-induction. Given this, we also conducted computational investigations into a scenario without alkali metal countercations, in which only hydrogen bonding interactions exist (Supplementary Fig. 26). The calculation results indicate that the relative Gibbs free energies of the two most advantageous transition states ***E-R*-TS$_{12}$** and ***Z-S*-TS$_{13}$** can be nearly identical, indicating very low enantioselectivity in this reaction. This aligns with the results of control experiments conducted in the presence of crown ether as the additive. Moreover, the energy differences of the calculated hydride transfer transition states for ethyl, methyl imine **1al**, and ethyl, *n*-propyl substrate **1b** correspond to the experimental enantioselectivity (Fig. 3d). Furthermore, the relative energies of the calculated hydride transfer transition states for both configurations are very similar when using phenyl-substituted **Mn-1** or 2-naphthyl **Mn-17** as the catalyst under the same conditions (Supplementary Fig. 28). These results align with the observed enantioselectivity trend in experiments (Fig. 3d). Further DFT calculations investigated the coordination mode of the ferrocenyl tridentate ligand on **Mn-13** catalyst with ethyl *n*-butyl imine **1a**. Analysing the comprehensive free-energy profiles showed the preference for facial coordination over meridional coordination throughout the catalytic cycle (Supplementary Figs. 32–34). Apart from computational mechanism studies, the formation of anionic manganese intermediates

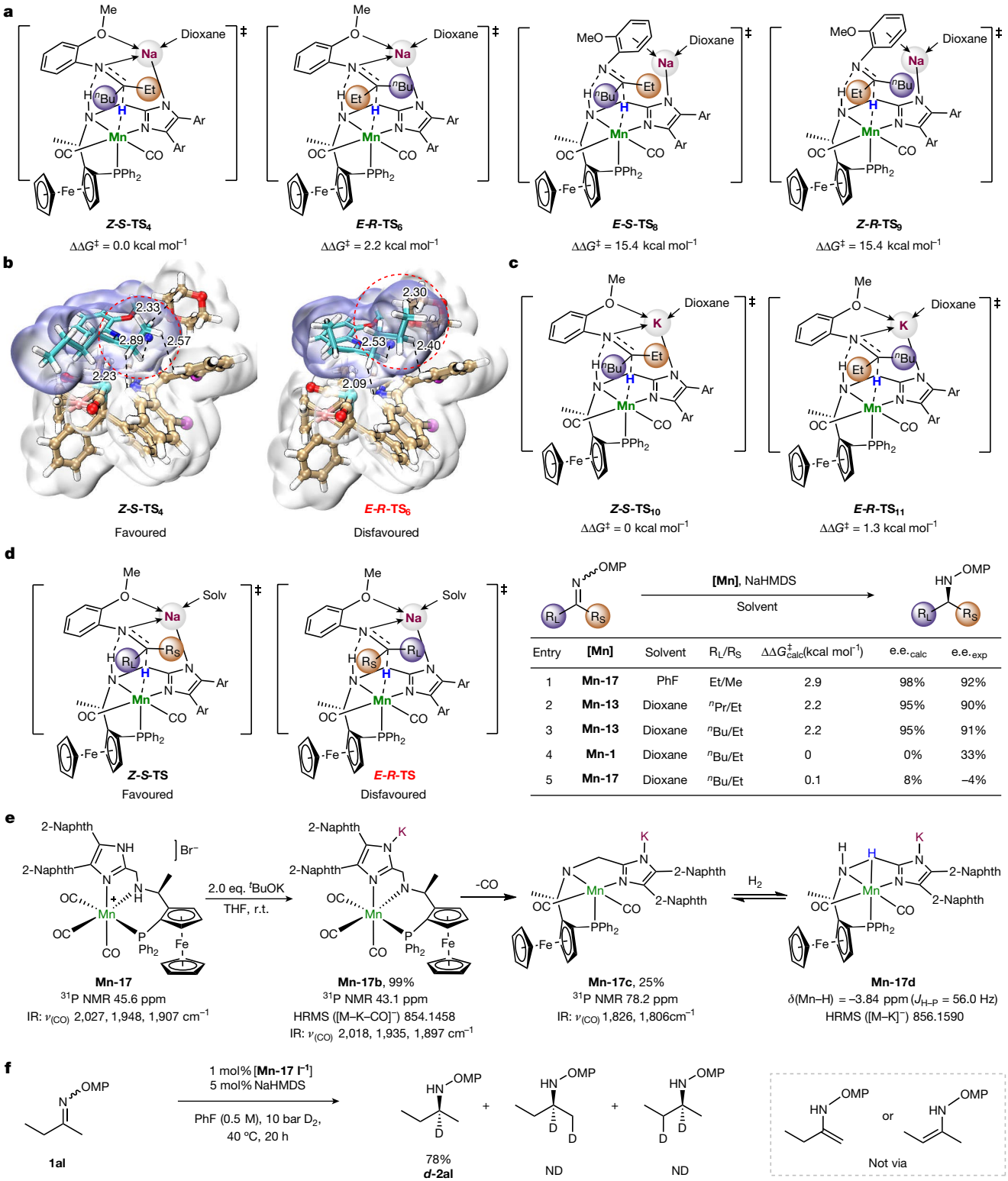

Fig. 3 | Mechanistic studies and DFT calculations. a, Four hydride transfer transition states involving sodium cations. For hydride transfer transition states by σ-coordination interactions, ***Z-S*-TS$_4$** is favoured over ***E-R*-TS$_6$** by 2.2 kcal mol^{-1}. For hydride transfer transition states by cation–π interactions, the energy barriers by ***E-S*-TS$_8$** and ***Z-R*-TS$_9$** are 15.4 kcal mol^{-1} higher than that by the favourable transition state ***Z*-S-TS$_4$**. **b**, van der Waals surface map of ethyl *n*-butyl imine; the van der Waals volume of ethyl is relatively small and can be accommodated by the confined reaction site. **c**, Hydride transfer transition states involving potassium cation. For hydride transfer transition state involving potassium cations, ***Z-S*-TS$_{10}$** is favoured over ***E-R*-TS$_{11}$** by 1.3 kcal mol^{-1}. **d**, Energy difference in hydride transfer transition states among different substrates and catalysts. **e**, Characterization of active anionic Mn species with **Mn-17**. **f**, Isotope labelling experiment. Ar = *o*-bromophenyl, r.t., room temperature. OMP =2-methoxyphenyl; r.t., room temperature.

was experimentally confirmed. Given the relative instability of the anionic amido manganese complex resulting from the reaction of **Mn-13** and ^{t}BuOK, **Mn-17** was chosen for further investigation because of the better stability of the corresponding generated complexes. Treating the amino manganese bromide complex **Mn-17** with 2.0 equivalents of ^{t}BuOK resulted in the generation of the corresponding anionic amido

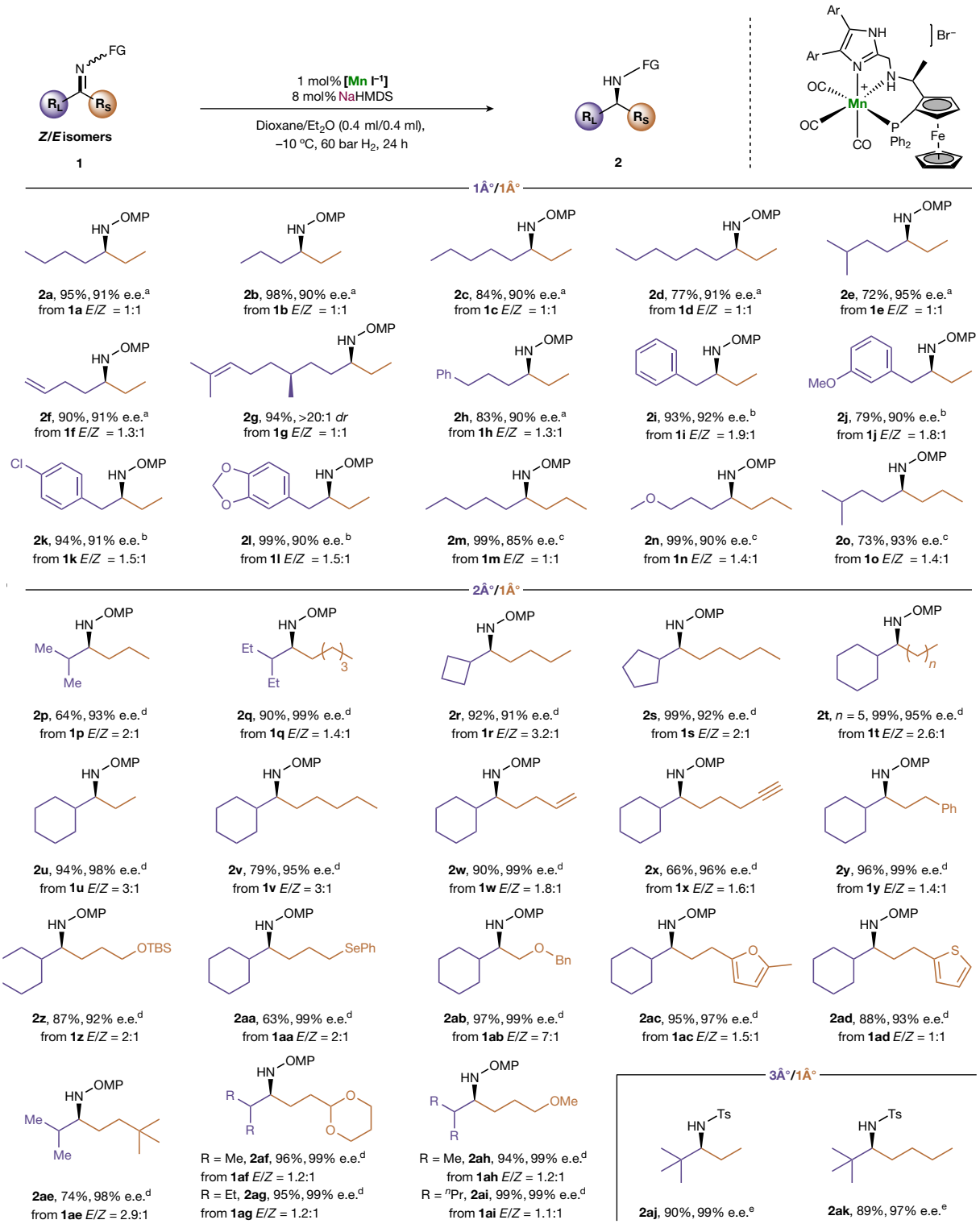

Fig. 4 | Substrate scope of imines with primary, secondary and tertiary alkyl and primary alkyl groups. [a]Reaction conditions: **1** (0.25 mmol), **Mn-13** (1 mol%), ligand (1 mol%) and NaHMDS (8 mol%) in a cosolvent of 1,4-dioxane (0.4 ml) and Et_2O (0.4 ml) at −10 °C for 20 h. Isolated yields (%) were given and enantioselectivities (% e.e.) were determined by chiral-phase high-performance liquid chromatography. [b]**Mn-19** (2 mol%) and KO^{t}Bu (10 mol%) in PhCl (0.8 ml) at 0 °C for 20 h. [c]**Mn-27** (1 mol%), (+)−2,2′-methylenebis[(3a*R*,8a*S*)−3a,8a-dihydro-8H-indeno[1,2-d]oxazole] (2.5 mol%), KO^{t}Bu (10 mol%) in Et_2O (1.6 mL) at −15 °C for 20 h. [d]**Mn-1** (2 mol%), and NaO^{t}Bu (10 mol%) in 1,4-dioxane (0.5 ml) at 60 °C for 16 h. [e]**Mn-1** (2 mol%), and ^{t}AmONa (1.0 eq.) in 1,4-dioxane (0.5 mL) at 50 °C for 16 h. OMP = 2-methoxyphenyl; FG, functional group.

manganese tricarbonyl complex **Mn-17b** in quantitative yield, which was characterized by ^{31}P nuclear magnetic resonance (NMR), infrared absorption spectrometry and high-resolution mass spectrometry (electrospray ionization) (HRMS (ESI)) analysis (Fig. 3e and Supplementary Figs. 7, 11 and 12). Following this, **Mn-17b** experienced a gradual loss of one molecule of CO, forming the corresponding anionic manganese dicarbonyl complex **Mn-17c** in low conversion. Subsequently, **Mn-17c** was subjected to a reaction with hydrogen, yielding the catalytically

active anionic manganese hydride species **Mn-17d**. ^{1}H NMR analysis of this reaction mixture revealed a doublet signal at δ = −3.84 ppm (J_{H-P} = 56.0 Hz), whereas HRMS (ESI) measurement detected a signal with an *m*/*z* value of 856.1590, representing the [M−K]$^-$ ion peak of **Mn-17d** (Supplementary Figs. 15 and 16). DFT calculations suggest that the basicity of ^{t}BuOK or NaHMDS is sufficient to further deprotonate the N–H group of **Mn-17d** and *fac*-**Int4**, resulting in the formation of anionic Mn–H complexes supported by dianionic ligands, **Mn-17e** and *fac*-**Int5**, respectively (Supplementary Fig. 29). However, the higher energy barrier for hydride transfer between *fac*-**Int5** and **1a** leads to *fac*-**Int5** becoming a thermodynamically stable off-cycle species (Extended Data Figs. 1 and 2). Furthermore, the deuterium labelling experiment eliminated the possibility of the reaction pathway involving the hydrogenation of enamine intermediates (Fig. 3f).

Reaction generality and utilities

With the optimized conditions established, we explored the scope concerning various imines (Fig. 4). As expected, the optimal catalytic system varied according to the class of substrates, ensuring precise discrimination among groups with different similarities. **Mn-13** emerged as a privileged catalyst for alkyl- and ethyl-substituted substrates. The ethyl group was effectively differentiated from longer *n*-alkyls and distal branched or functionalized alkyl groups (**2a**–**2h**). The desired products were obtained with good yields (72–98%) and excellent enantioselectivities (90–95% e.e.). Benzyl ethyl ketimines were also suitable substrates, yielding the corresponding products in 79–99% yields and 90–92% e.e. (**2i**–**2l**). For substrates with an *n*-propyl group (**1m**–**1o**), modified reaction conditions were used using **Mn-27** with a 3,5-di(*tert*-butyldiphenylsilyl)phenyl substituent (for detailed optimization, see Supplementary Table 5), resulting in good enantioselectivity (**2m**-**2o**, 85–93% ee.). The addition of a bisoxazoline ligand slightly improved the enantioselectivity of these transformations, probably attributed to their coordination with K^+ (ref. 40). In the case of ketimines bearing both secondary and primary alkyl groups, the substrates exhibited less sensitivity to reaction parameters, because of the increased differences in the steric hindrance. Satisfactory results were achieved by using the diphenyl-substituted complex **Mn-1** as the precatalyst. Imines substituted with secondary alkyls and primary alkyls of the same chain lengths yielded excellent outcomes (64–90% yields, 93–99% e.e., **2p**–**2t**). Good to excellent yields (63–99%) and high levels of enantioselectivity (92–99% e.e.) were achieved with substrates bearing various functional groups, such as alkenyl, alkynyl, phenyl, *tert*-butyldimethylsilyloxy, selenyl, benzyloxy, thienyl, furyl, *t*-butyl, 1,3-diohexyl-2-yl and methoxy groups (**2w**–**2ai**). For the hydrogenation of highly sterically hindered tertiary and primary alkyl imines with low reactivity, highly enantioselective transformations were realized under adjusted conditions (89-90% yields, 97–99% e.e., **2aj**–**2ak**), highlighting the remarkable reactivity of this catalytic system.

To further expand the substrate scope by the fine-tunability of the confined reaction site, we investigated the compatibility of primary alkyl/methyl ketimines. The substrate **1al**, derived from 2-butanone, represents another highly challenging substrate in the asymmetric hydrogenation reaction. After modifying the reaction conditions, it was observed that the naphthyl substituted **Mn-17** afforded the desired product **2al** in 91% yield with 92% e.e. (Extended Data Fig. 3). Substrates with different chain lengths and remote functional groups were tested under the optimal conditions, providing the corresponding chiral amines with excellent results, including analogues of amphetamine[41] (**2am**–**2au**, 90–95% e.e.). Building on our success with the above substrates, secondary or tertiary alkyl and methyl ketimines and aryl and alkyl imines were also investigated (Extended Data Fig. 3 and Supplementary Fig. 35). Excellent outcomes had also been achieved for these substrates (60–99% yields, 90–99% e.e.), highlighting the broad applicability of this approach to a wide range of imines. Furthermore, we proceeded to evaluate the robustness of this reaction system. The catalytic hydrogenation of **1as** was conducted at a low catalyst loading of 9 ppm on a gram scale (29.6 g, 110 mmol, S/*C* = 110,000:1, Extended Data Fig. 4). High enantioselectivity of the target product was maintained with an excellent turnover number of 107,800, setting a record number for the asymmetric hydrogenation enabled by Earth-abundant metal catalysis. To demonstrate the practicality of our methodology, we applied this catalytic system to the synthesis of several drugs and bioactive molecules (Extended Data Fig. 4). The chiral primary amine **3** was obtained with 61% yield by treating **2as** with periodic acid without the corrosion of enantiopurity, serving as an important intermediate in the synthesis of antiasthmatic drug (*R*,*S*)-formoterol[42]. Primary amine **4** (derived from **2aq**) facilitated a straightforward and efficient synthesis of (*S*)-levdobutamine through sequential condensation with (3,4-dimethoxyphenyl)acetic acid, reduction and demethylation. The MER tyrosine kinase inhibitor **8** (ref. 43) was prepared by the deprotection of **7** (derived from **2ab**) followed by condensation with nicotinic acid derivatives in two steps without loss of enantiopurity.

Beyond distinguishing between two similar alkyl groups, the significance of modular assembly, confined chiral catalysts lies in offering insights for the design of highly efficient catalysts in scenarios with intractable stereocontrol. By establishing multiple cooperative non-covalent attractive interactions between the substrate and the catalyst, along with confined reaction sites featuring fine-tunability, a high level of stereoselectivity control could be achieved in previously elusive asymmetric transformations.

Online content

Any methods, additional references, Nature Portfolio reporting summaries, source data, extended data, supplementary information, acknowledgements, peer review information; details of author contributions and competing interests; and statements of data and code availability are available at https://doi.org/10.1038/s41586-024-07581-z.

1. Walsh, P. J. & Kozlowski, M. C. *Fundamentals of Asymmetric Catalysis* (Univ. Science Books, 2010).
2. Zhang, F.-H., Zhang, F.-J., Li, M.-L., Xie, J.-H. & Zhou, Q.-L. Enantioselective hydrogenation of dialkyl ketones. *Nat. Catal.* **3**, 621–627 (2020).
3. Zhou, H. et al. Organocatalytic stereoselective cyanosilylation of small ketones. *Nature* **605**, 84–89 (2022).
4. McDaniel, D. H. & Brown, H. C. An extended table of Hammett substitutent constants based on the ionization of substituted benzoic acids. *J. Org. Chem.* **23**, 420–427 (1958).
5. Tolman, C. A. Steric effects of phosphorus ligands in organometallic chemistry and homogeneous catalysis. *Chem. Rev.* **77**, 313–348 (1977).
6. McFord, A. W., Butts, C. P., Fey, N. & Alder, R. W. 3× Axial vs 3× equatorial: the ΔG_{GA} value is a robust computational measure of substituent steric effects. *J. Am. Chem. Soc.* **143**, 13573–13578 (2021).
7. Bell, S. et al. Asymmetric hydrogenation of unfunctionalized, purely alkyl-substituted olefins. *Science* **311**, 642–644 (2006).
8. Li, C., Wang, C., Villa-Marcos, B. & Xiao, J. Chiral counteranion-aided asymmetric hydrogenation of acyclic imines. *J. Am. Chem. Soc.* **130**, 14450–14451 (2008).
9. Li, C., Villa-Marcos, B. & Xiao, J. Metal–Brønsted acid cooperative catalysis for asymmetric reductive amination. *J. Am. Chem. Soc.* **131**, 6967–6969 (2009).
10. Tang, W. et al. Cooperative catalysis: combining an achiral metal catalyst with a chiral Brønsted acid enables highly enantioselective hydrogenation of imines. *Chem. Eur. J.* **19**, 14187–14193 (2013).
11. Schramm, Y., Barrios-Landeros, F. & Pfaltz, A. Discovery of an iridacycle catalyst with improved reactivity and enantioselectivity in the hydrogenation of dialkyl ketimines. *Chem. Sci.* **4**, 2760–2766 (2013).
12. Bae, H. Y. et al. Approaching sub-ppm-level asymmetric organocatalysis of a highly challenging and scalable carbon-carbon bond forming reaction. *Nat. Chem.* **10**, 888–894 (2018).
13. Wang, Z., Yang, X.-Y., Xu, Y. & Zhou, Q.-L. Iridium-catalyzed asymmetric hydrogenation of dialkyl imines. *CCS Chem.* **6**, 905–911 (2024).
14. Yasukawa, T., Masuda, R. & Kobayashi, S. Development of heterogeneous catalyst systems for the continuous synthesis of chiral amines via asymmetric hydrogenation. *Nat. Catal.* **2**, 1088–1092 (2019).
15. Bahamonde, A., Al Rifaie, B., Martín-Heras, V., Allen, J. R. & Sigman, M. S. Enantioselective Markovnikov addition of carbamates to allylic alcohols for the construction of α-secondary and α-tertiary amines. *J. Am. Chem. Soc.* **141**, 8708–8711 (2019).
16. Xi, Y. et al. Application of Trimethylgermanyl-substituted bisphosphine ligands with enhanced dispersion interactions to copper-catalyzed hydroboration of disubstituted alkenes. *J. Am. Chem. Soc.* **142**, 18213–18222 (2020).

17. Knowles, R. R. & Jacobsen, E. N. Attractive noncovalent interactions in asymmetric catalysis: links between enzymes and small molecule catalysts. *Proc. Natl Acad. Sci. USA* **107**, 20678–20685 (2010).
18. Drauz, K., Gröger, H. & May, O. (eds) *Enzyme Catalysis in Organic Synthesis* (Wiley, 2012).
19. Savile, C. K., & Janey, J. M. Biocatalytic asymmetric synthesis of chiral amines from ketones applied to Sitagliptin manufacture. *Science* **329**, 305–309 (2010).
20. Reetz, M. T. Laboratory evolution of stereoselective enzymes: a prolific source of catalysts for asymmetric reactions. *Angew. Chem. Int. Ed.* **50**, 138–174 (2011).
21. Renata, H., Wang, Z. J. & Arnold, F. H. Expanding the enzyme universe: accessing non-natural reactions by mechanism-guided directed evolution. *Angew. Chem. Int. Ed.* **54**, 3351–3367 (2015).
22. Wang, Q.-Q. et al. Self-assembled nanospheres with multiple endohedral binding sites pre-organize catalysts and substrates for highly efficient reactions. *Nat. Chem.* **8**, 225–230 (2016).
23. Leenders, S. H. A. M., Gramage-Doria, R., de Bruin, B. & Reek, J. N. H. Transition metal catalysis in confined spaces. *Chem. Soc. Rev.* **44**, 433–448 (2015).
24. Mitschke, B., Turberg, M. & List, B. Confinement as a unifying element in selective catalysis. *Chem* **6**, 2515–2532 (2020).
25. Hou, G. et al. Enantioselective hydrogenation of N–H imines. *J. Am. Chem. Soc.* **131**, 9882–9883 (2009).
26. Zuo, W., Lough, A. J., Li, Y. F. & Morris, R. H. Amine(imine)diphosphine iron catalysts for asymmetric transfer hydrogenation of ketones and imines. *Science* **342**, 1080–1083 (2013).
27. Li, B., Chen, J., Liu, D., Gridnev, I. D. & Zhang, W. Nickel-catalysed asymmetric hydrogenation of oximes. *Nat. Chem.* **14**, 920–927 (2022).
28. Mas-Roselló, J., Smejkal, T. & Cramer, N. Iridium-catalyzed acid-assisted asymmetric hydrogenation of oximes to hydroxylamines. *Science* **368**, 1098–1102 (2020).
29. Oates, C. L., Goodfellow, A. S., Bühl, M. & Clarke, M. L. Manganese catalysed enantioselective hydrogenation of *in situ*-synthesised imines: efficient asymmetric synthesis of amino-indane derivatives. *Green Chem.* **25**, 3864–3868 (2023).
30. Chen, J.-J. et al. Enantioconvergent Cu-catalysed N-alkylation of aliphatic amines. *Nature* **618**, 294–300 (2023).
31. Xi, Y., Ma, S. & Hartwig, J. F. Catalytic asymmetric addition of an amine N-H bond across internal alkenes. *Nature* **588**, 254–260 (2020).
32. Yang, Y., Shi, S.-L., Niu, D., Liu, P. & Buchwald, S. L. Catalytic asymmetric hydroamination of unactivated internal olefins to aliphatic amines. *Science* **349**, 62–66 (2015).
33. Friedfeld, M. R., Zhong, H., Ruck, R. T., Shevlin, M. & Chirik, P. J. Cobalt-catalyzed asymmetric hydrogenation of enamides enabled by single-electron reduction. *Science* **360**, 888–893 (2018).
34. Wang, Y. et al. Structure, reactivity and catalytic properties of manganese-hydride amidate complexes. *Nat. Chem.* **14**, 1233–1241 (2022).
35. Freitag, F., Irrgang, T. & Kempe, R. Mechanistic studies of hydride transfer to imines from a highly active and chemoselective manganate catalyst. *J. Am. Chem. Soc.* **141**, 11677–11685 (2019).
36. Wen, J., Wang, F. & Zhang, X. Asymmetric hydrogenation catalyzed by first-row transition metal complexes. *Chem. Soc. Rev.* **50**, 3211–3237 (2021).
37. Garbe, M. et al. Manganese(I)-catalyzed enantioselective hydrogenation of ketones using a defined chiral PNP pincer ligand. *Angew. Chem. Int. Ed.* **56**, 11237–11241 (2017).
38. Widegren, M. B., Harkness, G. J., Slawin, A. M. Z., Cordes, D. B. & Clarke, M. L. A highly active manganese catalyst for enantioselective ketone and ester hydrogenation. *Angew. Chem. Int. Ed.* **56**, 5825–5828 (2017).
39. Liu, C., Liu, X. & Liu, Q. Stereodivergent asymmetric hydrogenation of quinoxalines. *Chem* **9**, 2585–2600 (2023).
40. Yamashita, Y., Noguchi, A., Fushimi, S., Hatanaka, M. & Kobayashi, S. Chiral metal salts as ligands for catalytic asymmetric Mannich reactions with simple amides. *J. Am. Chem. Soc.* **143**, 5598–5604 (2021).
41. Huang, H., Liu, X., Zhou, L., Chang, M. & Zhang, X. Direct Asymmetric reductive amination for the synthesis of chiral *β*-arylamines. *Angew. Chem. Int. Ed.* **55**, 5309–5312 (2016).
42. Murakami, M., Takahashi, K., Mase, T., Murase, K. & Ida, H. *α*-Aminomethylbenzyl alcohol derivatives. US patent 3,994,974 (1976).
43. Kim, M.-S. et al. Heteroaryl compounds and their use as therapeutic drugs. Patent WO2017039331 (2017).

Data availability

All data are available in the main text or the supplementary materials.

Acknowledgements We thank Y. Xi from the National University of Singapore and J. Xiao from the University of Liverpool for helpful discussions and valuable revisions. Financial support from the National Key R&D Program of China (2021YFF0701600) and the National Natural Science Foundation of China (22225103 and 22171159) is greatly appreciated.

Author contributions M.W., Y.L. and Q.L. did the conceptualization of the study. M.W., S.L. and H.L. contributed to the methodology. M.W., S.L. and H.L. did the investigation. Y.L. and Q.L. were involved in funding acquisition. Y.L. and Q.L. did the project administration. Y.L. and Q.L. supervised the work. M.W., S.L., Y.W. and Q.L. wrote the original draft. M.W., Y.L. and Q.L. contributed to the writing, review and editing of the paper.

Competing interests The authors declare no competing interests.

Additional information

Supplementary information The online version contains supplementary material available at https://doi.org/10.1038/s41586-024-07581-z.

Correspondence and requests for materials should be addressed to Yu Lan or Qiang Liu.

Peer review information *Nature* thanks Rhett Kempe and the other, anonymous, reviewer(s) for their contribution to the peer review of this work.

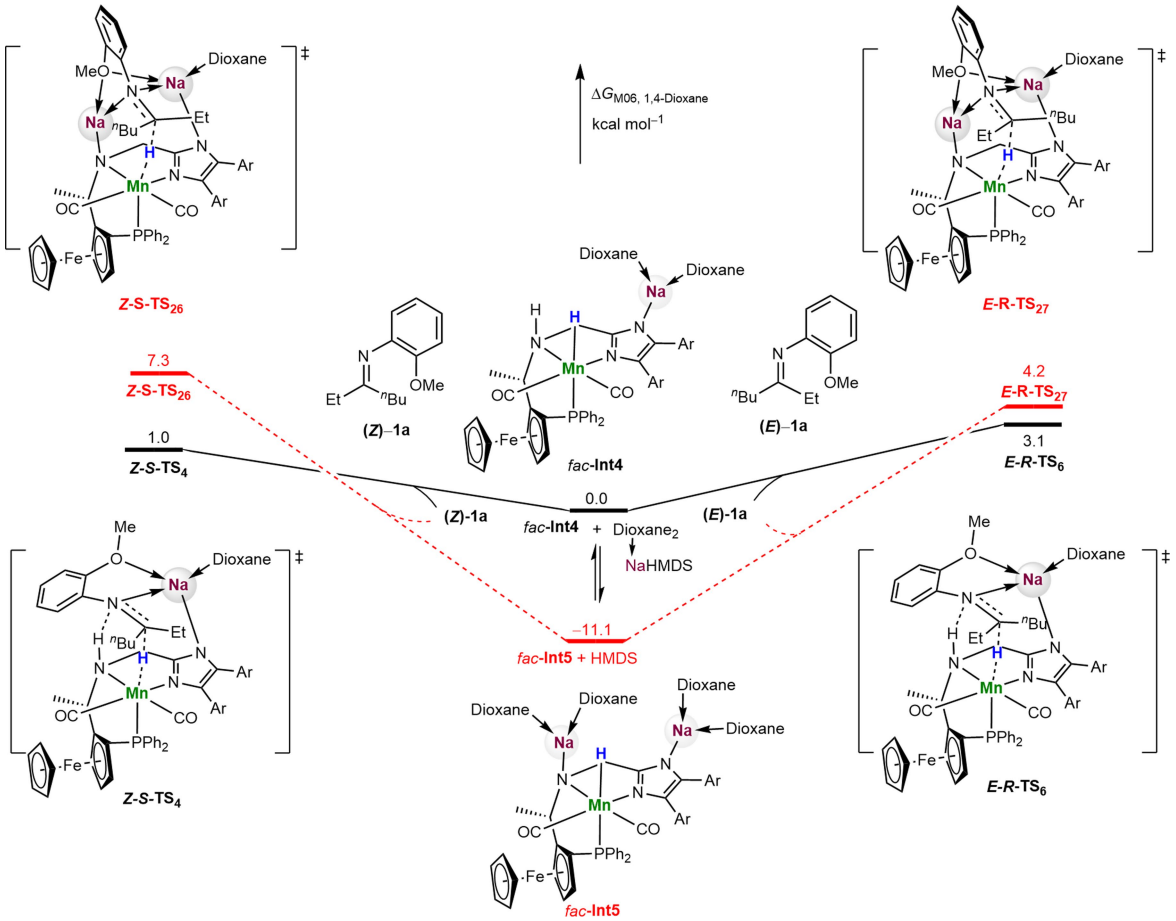

Extended Data Fig. 1 | Comparison of free energy profiles. Free energy profiles for the hydride transfer of **1a** promoted by *fac*-**Int4** and *fac*-**Int5**. Ar = *o*-bromophenyl.

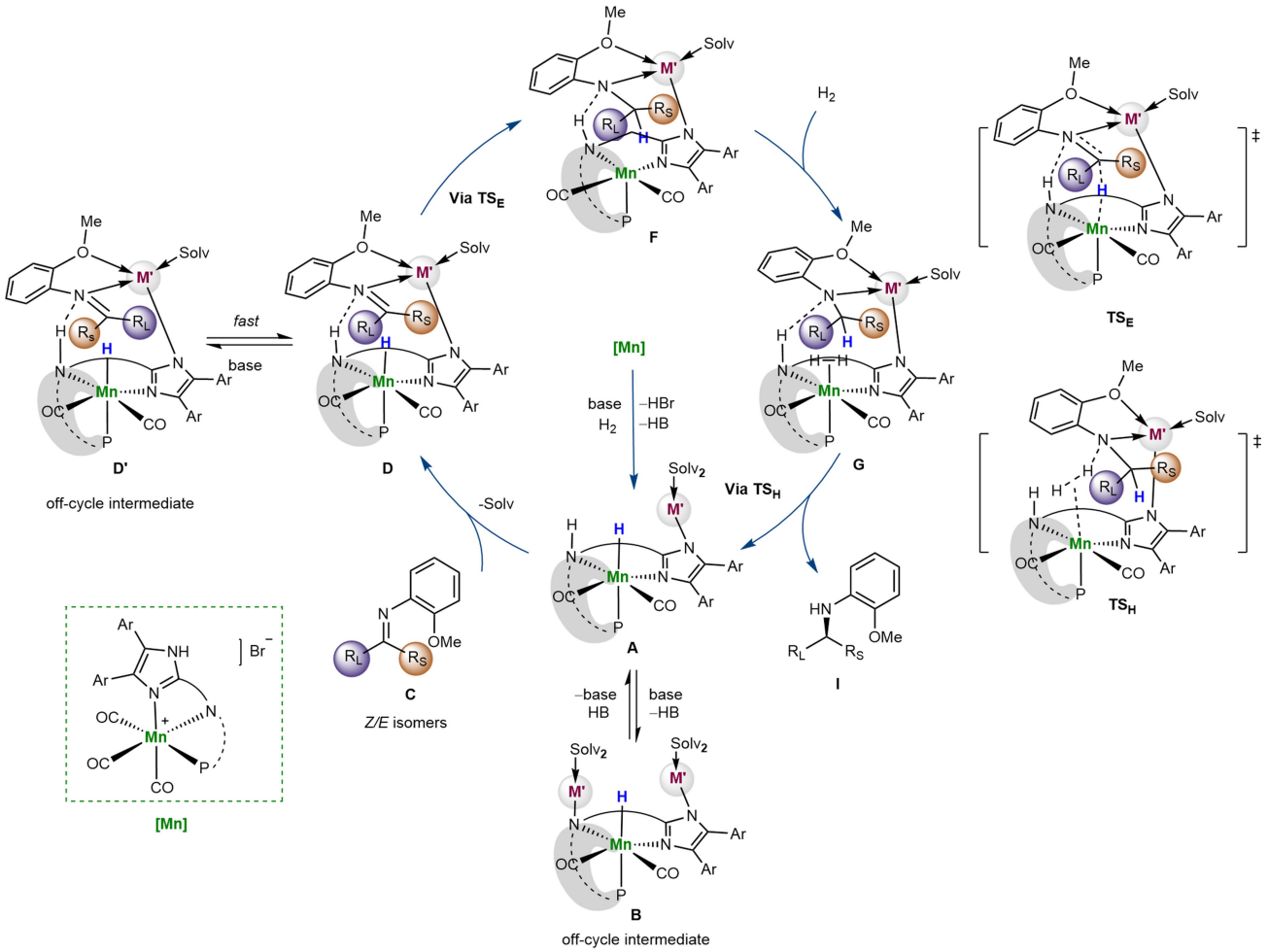

Extended Data Fig. 2 | Catalytic cycle. Proposed mechanism for the Mn-Catalyzed asymmetric hydrogenation of ketimines.

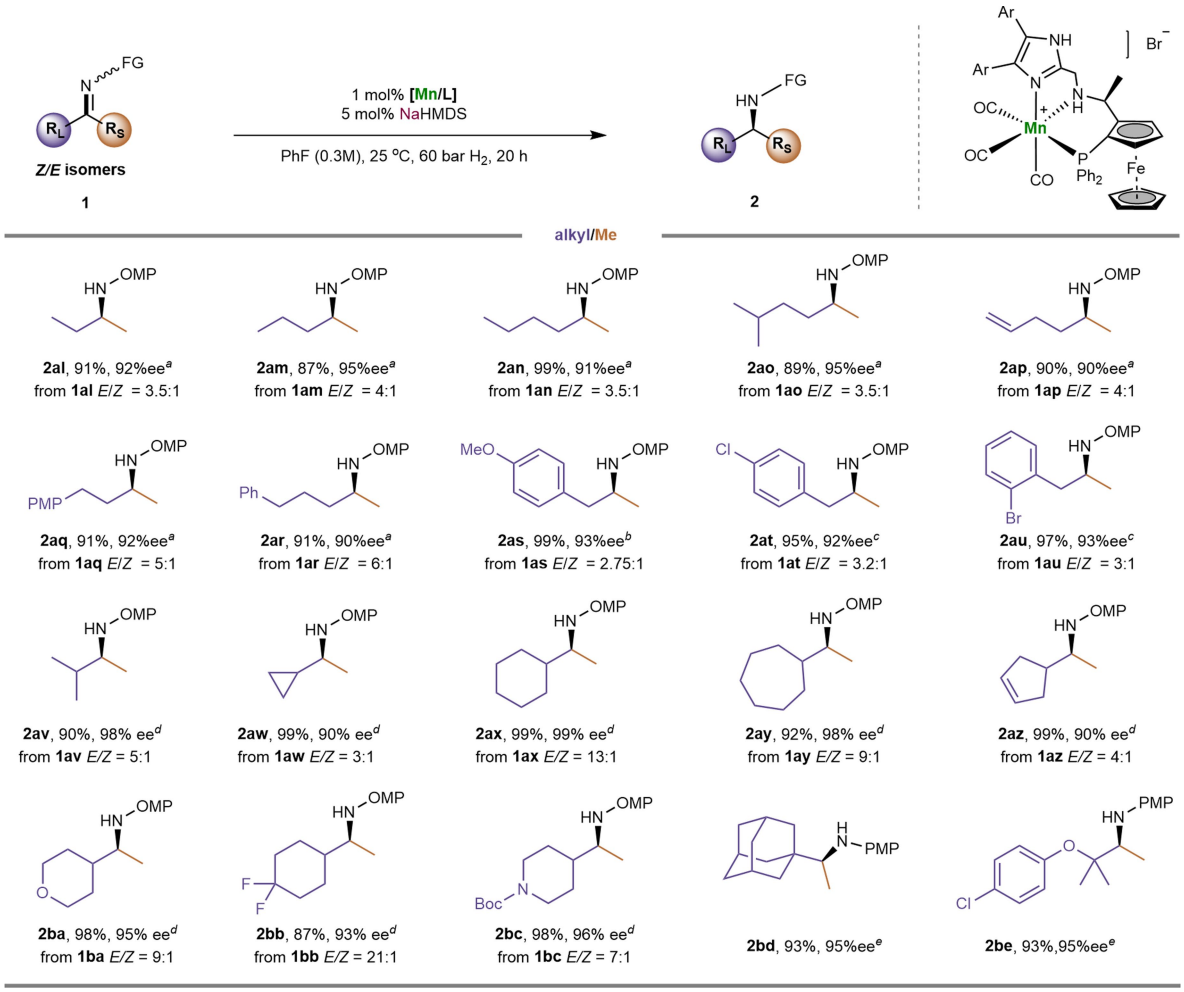

Extended Data Fig. 3 | Substrate scope of imines with primary/secondary/tertiary alkyl and methyl groups. [a]Reaction conditions: **1** (0.25 mmol), **Mn-17** (2 mol%) and NaHMDS (5 mol%) in PhF (0.5 mL) at 5 °C for 20 h. Isolated yields (%) were given and enantioselectivities (%*ee*) were determined by chiral-phase HPLC. [b]**Mn-15** was used instead of **Mn-17** at 25 °C. [c]**Mn-6** was used instead of **Mn-17** at 25 °C. [d]**Mn-1** (2 mol%) and NaO^{t}Bu (10 mol%) in 1,4-dioxane (0.8 mL) at 60 °C for 20 h. [e]**Mn-1** (2 mol%) and KO^{t}Bu (20 mol%) in diethylene glycol dimethyl ether (0.8 mL) at 25 °C.

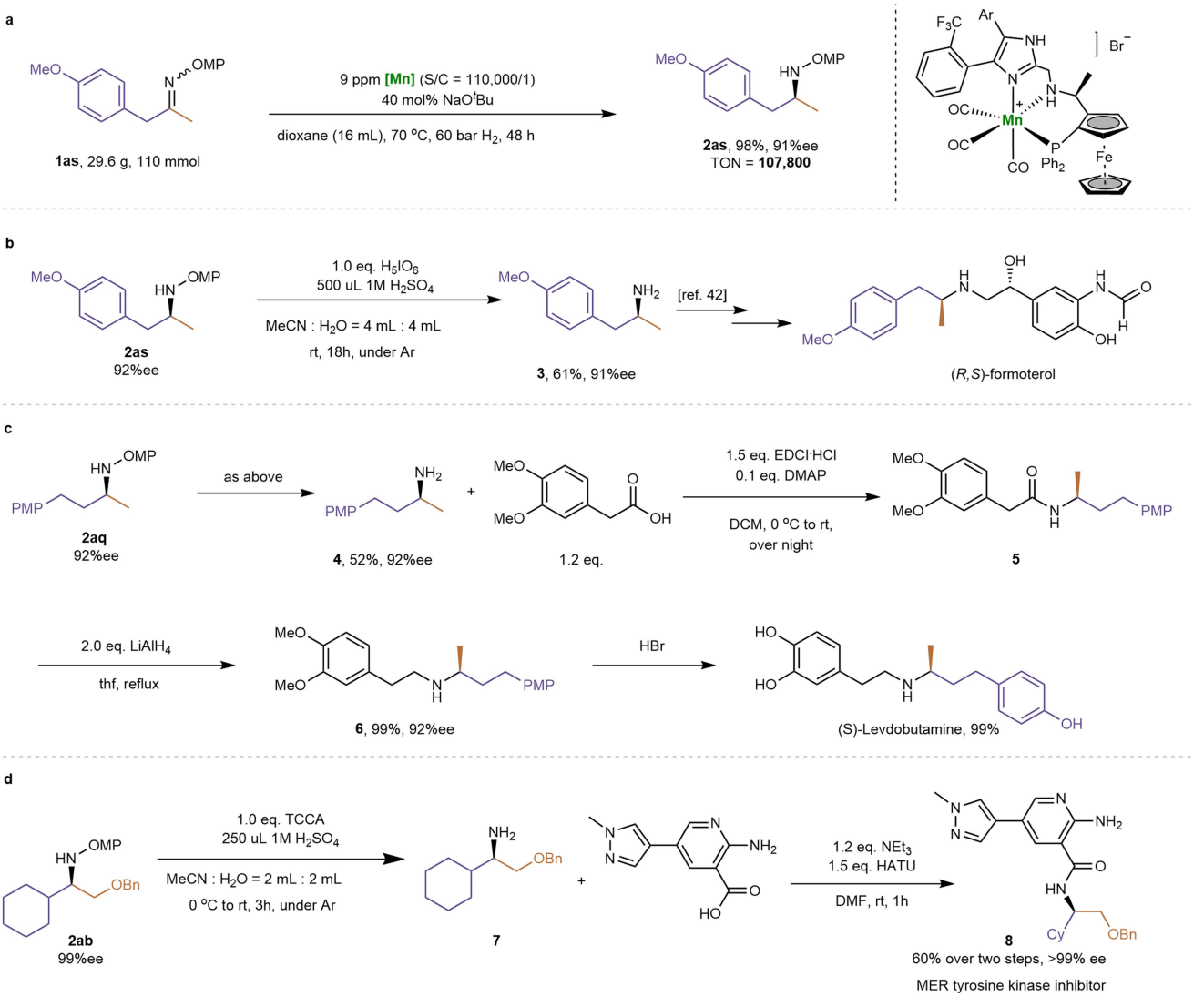

Extended Data Fig. 4 | Synthetic applications. a, Test of catalytic activity, TON experiment on a scale of grams. **b**, Deprotection of *N*-PG for the synthesis of primary amine. **c**, Preparation of (*S*)-Levdobutamine. **d**, Preparation of bioactive MER tyrosine kinase inhibitor (TCCA = trichloroisocyanuric acid; HATU = 2-(7-azabenzotriazol-1-yl)-*N*,*N*,*N*′,*N*′-tetramethyluronium hexafluorophosphate).